AGU PUBLICATIONS

JGR

Journal of Geophysical Research: Space Physics

RESEARCH ARTICLE
10.1002/2015JA022273

Key Points:
- Equatorward and eastward MSTIDs propagation
- Occurrence characteristics of MSTIDs
- Possible connection between the observed MSTIDs and AGW

Correspondence to:
O. F. Jonah,
olusegun.jonah@inpe.br

Citation:
Jonah, O. F., E. A. Kherani, and E. R. De Paula (2016), Observation of TEC perturbation associated with medium-scale traveling ionospheric disturbance and possible seeding mechanism of atmospheric gravity wave at a Brazilian sector, *J. Geophys. Res. Space Physics*, *121*, doi:10.1002/2015JA022273.

Received 14 DEC 2015
Accepted 15 FEB 2016
Accepted article online 18 FEB 2016

Observation of TEC perturbation associated with medium-scale traveling ionospheric disturbance and possible seeding mechanism of atmospheric gravity wave at a Brazilian sector

O. F. Jonah[1], E. A. Kherani[1], and E. R. De Paula[1]

[1]National Institute for Space Research (INPE), São Paulo, Brazil

Abstract In the present study, we document daytime total electron content (TEC) disturbances associated with medium-scale traveling ionospheric disturbances (MSTIDs), on few chosen geomagnetically quiet days over Southern Hemisphere of Brazilian longitude sector. These disturbances are derived from TEC data obtained using Global Navigation Satellite System (GNSS) receiver networks. From the keograms and cross-correlation maps, the TEC disturbances are identified as the MSTIDs that are propagating equatorward-eastward, having most of their average wavelengths longer in latitude than in longitude direction. These are the important outcomes of the present study which suggest that the daytime MSTIDs over Southern Hemisphere are similar to their counterparts in the Northern Hemisphere. Another important outcome is that the occurrence characteristics of these MSTIDs and that of atmospheric gravity wave (AGW) activities in the thermosphere are found to be similar on day-to-day basis. This suggests a possible connection between them, confirming the widely accepted AGW forcing mechanism for the generation of these daytime MSTIDs. The source of this AGW is investigated using the Geostationary Operational Environmental Satellite system (GOES) and Constellation Observing System for Meteorology, Ionosphere, and Climate satellite data. Finally, we provided evidences that AGWs are generated by convection activities from the tropospheric region.

1. Introduction

Medium-scale traveling ionospheric disturbances (MSTIDs) are the wave-like disturbances in the ionospheric density that travel through the ionosphere over very long distance covering high to low latitudes [*Hines*, 1960; *Bristow and Greenwald*, 1996; *Oliver et al.*, 1997; *Nicolls and Kelley*, 2005]. Several authors [*Wanninger*, 2004; *Chen et al.*, 2003] have shown that despite the small amplitude of MSTIDs (typically of tenths of a TECU), its presence could cause a decrease (sometime dramatic) on the performance of the precise navigation strategies since high precision is needed in the ionospheric interpolation and predictions. MSTIDs have wavelength between 100 and 500 km, time period between 15 and 60 min, and the phase speed of order of 50–400 m/s. Daytime MSTIDs are typically associated with atmospheric gravity waves [*Hines*, 1960], while nighttime MSTIDs are often associated with electrodynamics processes (which may be seeded by AGWs) [*Kelley*, 2011; *Miller et al.*, 2014]. The MSTIDs activities and amplitudes vary depending on latitude, longitude, local time, season, and solar cycle [*Kotake et al.*, 2006; *Hernandez-Pajares et al.*, 2006].

Daytime MSTIDs have been observed using various techniques such as ionosondes, high-frequency (HF) Doppler sounders, satellite beacons, and incoherent scatter radars [*Hocke and Schlegel*, 1996]. With the rapid advance in satellite technique in recent years, the global coverage of ionosphere brought an opportunity to study these MSTIDs in great detail [e.g., *Tsugawa et al.*, 2007; *Otsuka et al.*, 2011, 2013; *Hernandez-Pajares et al.*, 2006, 2012]. With the dense Global Navigation Satellite System (GNSS) receiver network over Northern Hemisphere, these studies have revealed the finer details of MSTIDs such as (a) their amplitudes which can be as large as 10% of the background, (b) their preferred direction of propagation toward equatorward-eastward (daytime) and equatorward-westward (nighttime) in the Southern and Northern Hemispheres, respectively, and (c) their association with the AGW activities and electrodynamics processes.

While there have been few studies of daytime MSTIDs using the GNSS receiver network [e.g., *Hernandez-Pajares et al.*, 2006, 2012; *MacDougall and Jayachandran*, 2011; *Grocott et al.*, 2013], most of the studies over Southern Hemisphere (e.g., Brazil) have been limited to the nighttime MSTIDs observed using the all-sky imagers [*Pimenta et al.*, 2008; *Candido et al.*, 2008; *Amorim et al.*, 2011]. Unlike Northern Hemisphere, over most

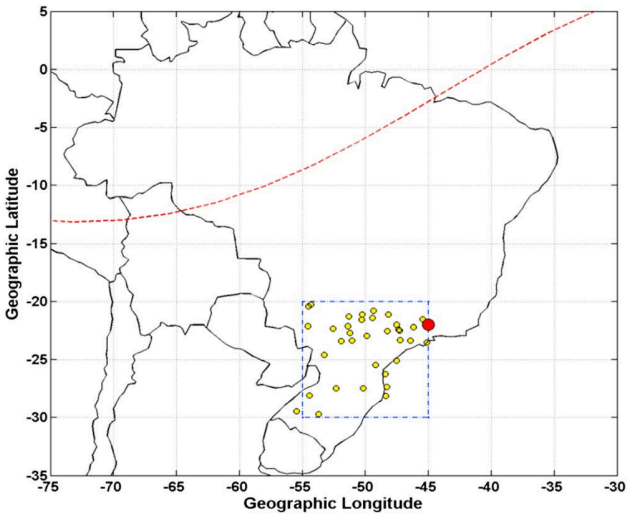

Figure 1. The yellow circles show the distribution of the GPS receivers used, the red circle shows the station of the ionogram location, and the red dashed line shows the magnetic field line.

parts of the Southern Hemisphere, the detailed features of daytime MSTIDs are not reported mainly due to the limited spatial resolution of the GNSS network. In recent years, with improved spatial resolution of GNSS over Brazil, varieties of large-scale ionospheric phenomena such as the four wave structures and TEC variability over South American sector [*Nogueira et al.*, 2013; *Jonah et al.*, 2015], TEC disturbances during Sudden Stratospheric Warming (SSW) [*Jonah et al.*, 2014; *Paes et al.*, 2014], and medium-scale phenomena such as the plasma bubbles [*Takahashi et al.*, 2014] have been reported using the GNSS technology. These studies have given a direction to further explore the possibility of identifying the MSTIDs from the TEC measurements. In the present study, we aim to present the TEC measurements on few chosen geomagnetic quiet days and derive the TEC disturbance. While TIDs are known to be manifestation of AGW, the sources of this AGW are not yet established. In this study we show (by using the experimental data provided by GOES and Constellation Observing System for Meteorology, Ionosphere, and Climate (COSMIC) satellite) the tropospheric cloud convection as a possible forcing mechanism for AGW causing the observed MSTIDs. We further adopt a methodology dealing with the cross-correlation maps that enable us to identify the MSTIDs from the derived TEC disturbances. Our results have been compared with relevant literatures over Southern Hemisphere [*Hernandez-Pajares et al.*, 2006, 2012] using perturbed GPS-TEC at one New Zealand sector (43.8°S–43.3°S and 169.5°E–170.5°E) and *MacDougall and Jayachandran* [2011] using digisonde data over the Brazilian equatorial region and they show good agreement.

2. Data and Method Used

In this study, we made use of the following experimental data from GNSS receivers, digisonde, GOES, and COSMIC satellite data.

1. The GNSS data are used to obtain detrended TEC, and consequently, the MSTIDs were obtained from Scripts and Permanent Array Centre Garner GPS archive and Brazilian Network for Continuous Monitoring of the Institute of Brazilian Geography and Statistics (RBMC/IBGE). The data are available at ftp://garner.ucsd.edu/pub/rinex/ and ftp://geoftp.ibge.gov.br/RBMC/dados/, respectively. The distribution of the GNSS data is given by yellow circles as represented in Figure 1.
2. The digisonde data are used to investigate the AGW signature during the observed MSTIDs propagation in order to verify the downward phase motion of two frequencies [*Lanchester et al.*, 1993]. The data were provided by the National Institute for Space Research (INPE). The position of the digisonde is shown by red circle at Figure 1.
3. Geostationary Operational Environmental Satellite system (GOES) supports weather forecasting, severe storm tracking, and meteorology research. In this study the GOES 13 satellite is used to observe the cloud convection activities. The data can be obtained at http://satelite.cptec.inpe.br/acervo/goes.formulario.logic?i=br#.
4. Constellation Observing System for Meteorology, Ionosphere, and Climate (COSMIC) is a program designed to provide advances in meteorology, ionospheric research, climatology, and space weather by using GPS satellites in conjunction with low Earth orbiting satellites. The mission is operated jointly by both U.S.-Taiwan. We used the COSMIC data to obtain the temperature profile to observe some characteristics of AGW during the MSTIDs event days. The data can be obtained from "http://tacc.cwb.gov.tw/cdaac/products.html."
5. The geomagnetic activity measured by *Kp* index which was < 3 during the period of study. The data were obtained from the Data Analysis Center for Geomagnetism and Space Magnetism at World Data Center for Geomagnetism, Kyoto, data base (http://wdc.kugi.kyoto-u.ac.jp/index.html).

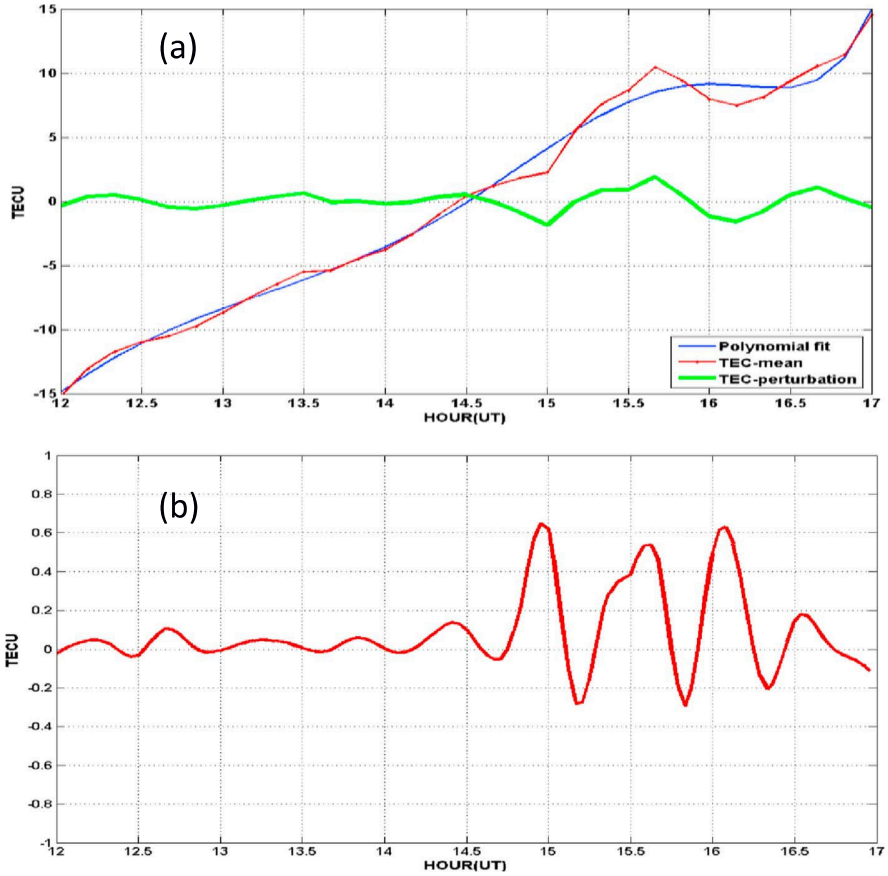

Figure 2. (a) TEC mean (red color), its polynomial fit (blue color), and the resultant detrended TEC, while (b) the red curve shows an example of the cross correlation between two latitude which represents the MSTID propagation.

2.1. Estimation of Delta TEC and Corresponding Correlation Maps

The Nagoya model [*Otsuka et al.*, 2002] is employed to derive the absolute TEC map over a chosen region (30° – 20°S and 45° – 55°W) which has relatively high GNSS receiver spatial resolution of order of 200 km. We focus on the TEC measurements during 12–17 UT. From this TEC map, keograms are generated by choosing a cut along latitude and a cut along longitude directions. These keograms consist of the temporal variation of TEC distributed along the latitude and longitude. A polynomial fit with order 7 is employed to each of these spatially distributed time series and corresponding best fits are obtained. From this, the TEC disturbance (ΔTEC) is derived by subtracting the TEC best fit (TEC_{fit}) from the TEC mean; i.e.,

$$\Delta\,\mathrm{TEC} = \overline{\mathrm{TEC}_i} - \mathrm{TEC}_{\mathrm{fit}}(x,t) \tag{1}$$

where $\overline{\mathrm{TEC}_i} = \frac{\sum_{t=1}^{N} \mathrm{TEC}_t}{N}$, i represents each latitude or longitude for all time, and N is the total number of t. InFigure 2a the blue and red curves represent the polynomial fit and the mean TEC, respectively, while the green curve is the detrended TEC obtained by equation (1). This method of deriving ΔTEC has been earlier employed by *Galvan et al.* [2011] to identify the tsunamigenic TEC disturbances and TIDs.

From these keograms of ΔTEC, cross-correlation maps are generated. The cross correlation is defined as follows:

$$\mathrm{MSTID}_{\mathrm{PROP}} = \frac{\Delta\,\mathrm{TEC}(x,t)\times\Delta\,\mathrm{TEC}(x+\Delta x, t+\Delta t)}{(\Delta\,\mathrm{TEC})^2} \tag{2}$$

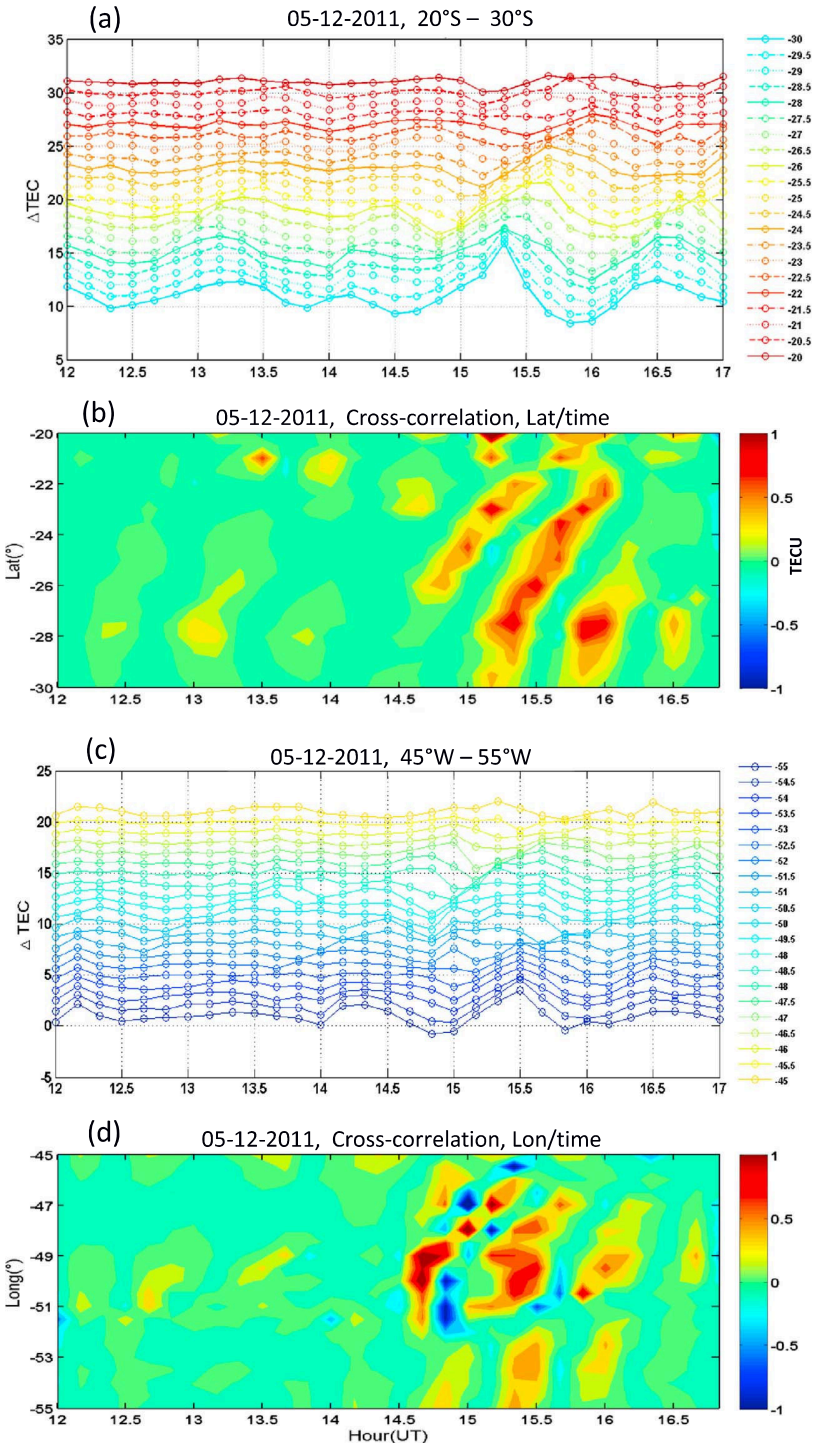

Figure 3. (a and c) The TEC disturbance. Each line represents latitude and longitude as indicated in the legends respectively. (b and d) MSTID propagation derived from the cross-correlation coefficients in latitude and longitude, respectively.

where x is the space (in longitude or latitude), $(\Delta x, t)$ is change in space with time, and $\mathrm{MSTID}_{\mathrm{PROP}}$ is the cross-correlation coefficient. These cross-correlation maps enable us to identify the waves, if present, by tracking the space and temporal shift of the maximum cross-correlation region. An example of this cross correlation is shown in Figure 2b which represents the MSTIDs propagation between two latitudes as represented by equation (2).

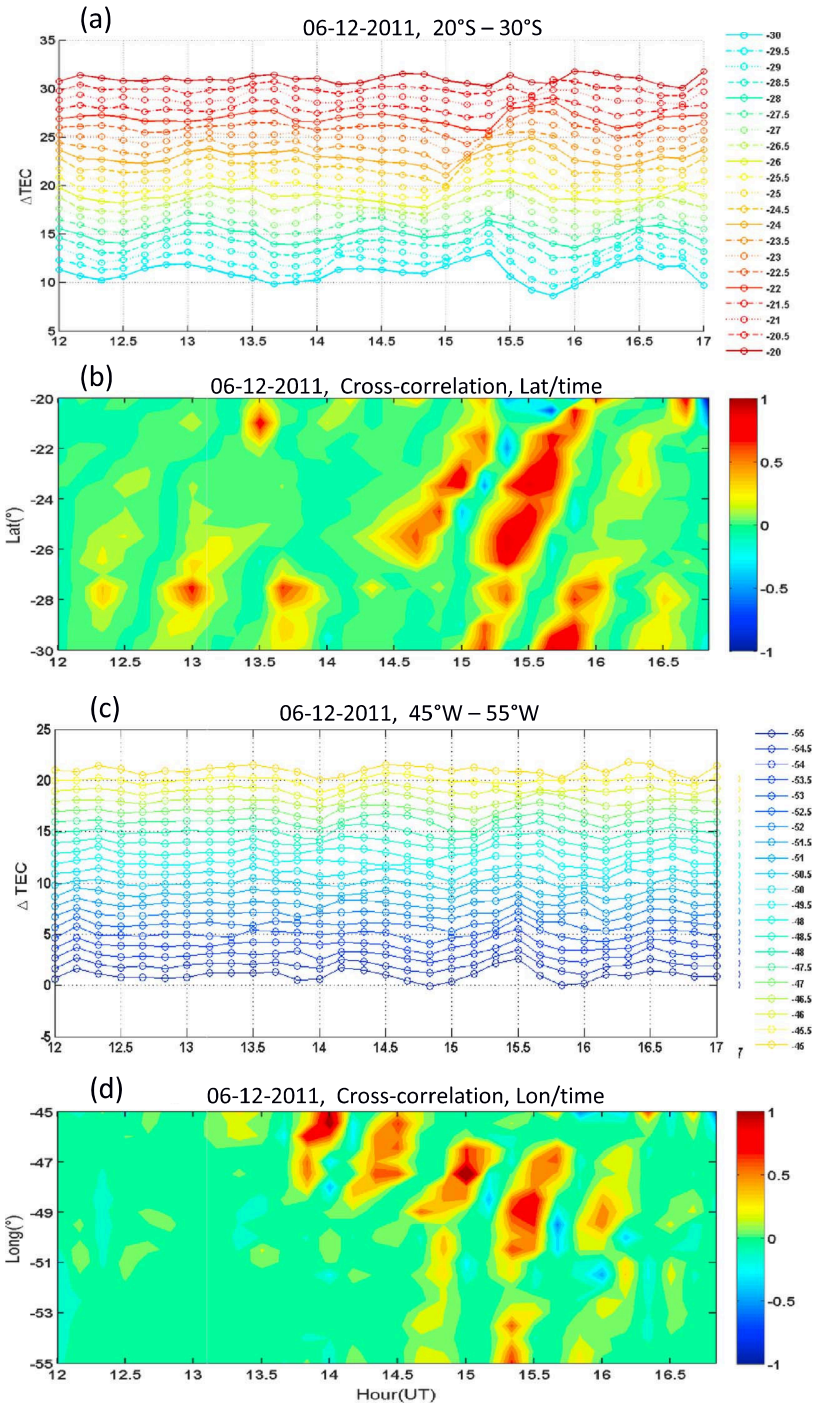

Figure 4. The same as Figure 3 but for day 6.

In the statistical analyzes the following methods are used:

We represent an event as a single wave (i.e., each high and low peak in time) for each day. In each day 10–14 events are identified depending on the MSTIDs activities for both latitude and longitude. The MSTIDs are defined as the TEC perturbations with amplitude greater than 0.2 total electron content unit (TECU, 1 TECU = 10^{16} electron/m^2) and period of perturbation less than 60 min. The statistical analyses are computed using the following steps:

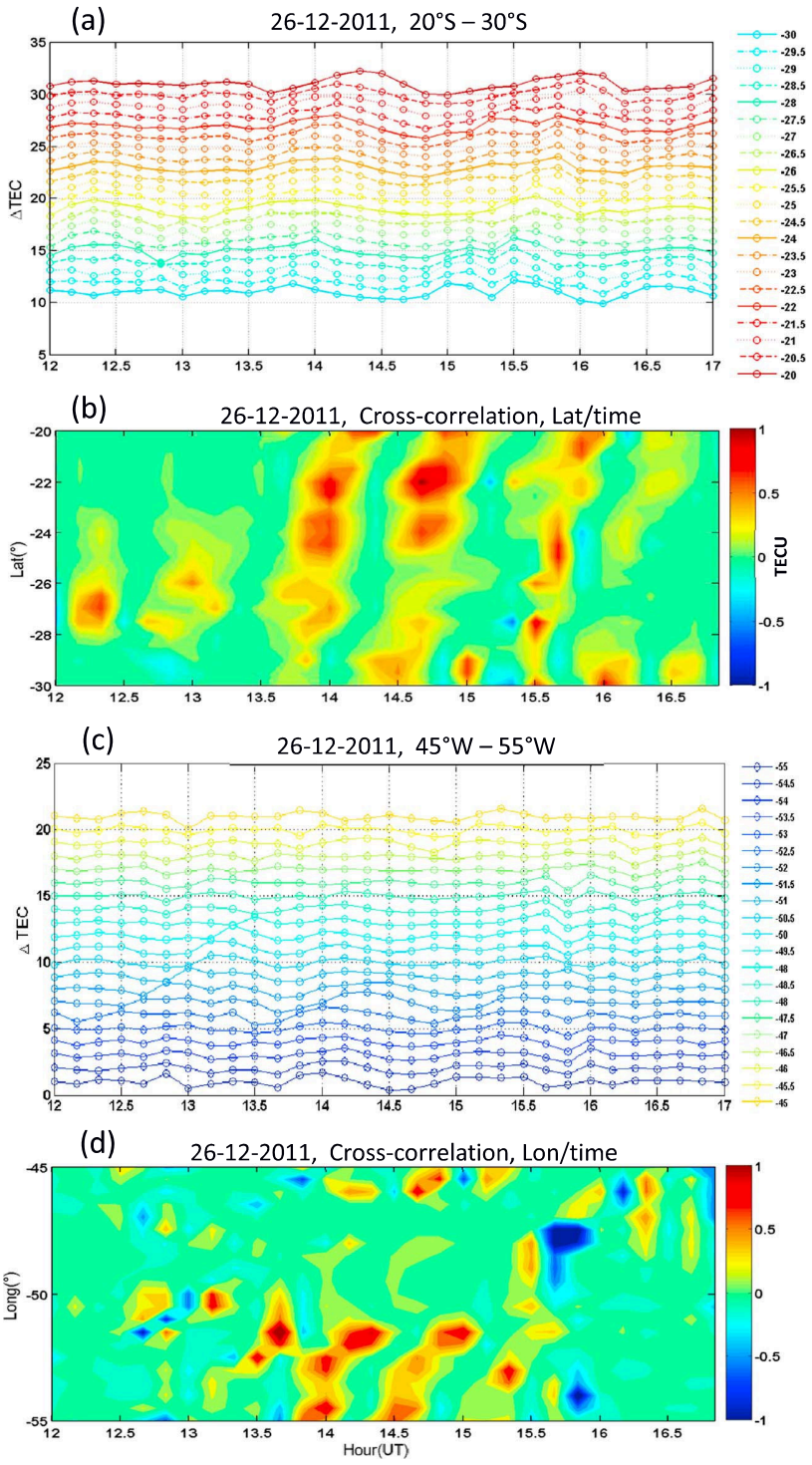

Figure 5. The same as Figure 3 but for day 26.

1. To calculate the period of each wave event, a peak to peak wave in time was defined as one wave period.
2. The velocity of the wave were computed by using the basic wave relations; i.e., the velocity is the distance (λ) the wave traveled in space (latitude or longitude) divided by the time interval (i.e., $V = \lambda/T$), where λ is the wavelength and the T is the period of the MSTIDs.

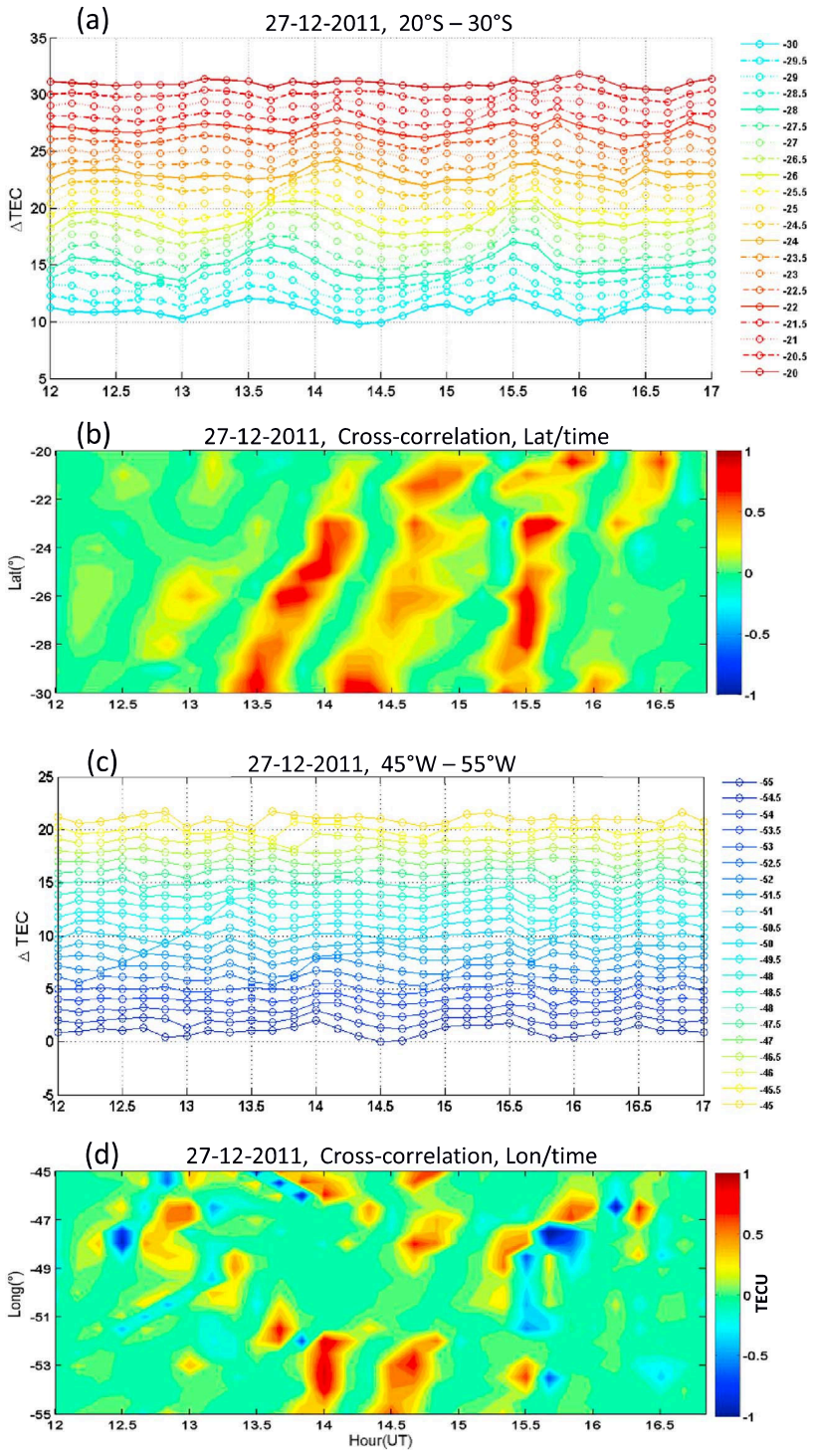

Figure 6. The same as Figure 3 but for day 27.

3. The wavelength is defined as the distance between peak to peak of the each wave event using visual assessment of the TEC perturbation map.
4. The orientation and propagation direction of the each wave is determined by the ratio between the vertical and horizontal wavelength. While the vertical wavelength (λ_x) is related to the wave observed

in the latitude and given by $2\pi/k_x$, the horizontal wavelength (λ_y) is related to the wave observed in the longitude and is given by $2\pi/k_x$. Hence, the propagation direction is defined as $\tan\theta = \lambda_x/\lambda_y = k_y/k_x$, where k_x and k_y are the wave numbers in latitude and longitude, respectively.

3. Results

Figures 3a–3d present the derived ΔTEC disturbances from the GNSS measurements during quiet geomagnetic conditions on 5 December 2011 during 12–17 UT. Figures 3a and 3c (derived by equation (1)), depict the temporal variation of the disturbances extracted between 30° − 20°S and 45° − 55°W, and the corresponding keograms of cross-correlation map in latitude and longitude (derived using equation (2)) are represented by Figures 3b and 3d, respectively. Figures 4a–4d and 6a–6d represent the same corresponding parameters but for 6, 26, and 27 December 2011. For easy comprehensive discussion, we refer 5, 6, 26, and 27 December 2011 as D5, D6, D26, and D27.

We note the following features in Figures 3a–3d on D5: (a) ΔTEC disturbance oscillates in time at a chosen location with periods covering between 20 and 55 min, (b) the phase of the oscillation shifts in time while going toward equator and eastward, (c) corresponding cross correlations maximize sometime during 13–16 UT, (d) the maxima are observed to commonly shift toward equatorward/eastward with time, (e) these cross-correlation maxima shifts longer and last longer in latitude than in longitude. Qualitatively, similar features are noted during D6, D26, and D27 at Figures 4, 5, and 6, respectively. Noteworthy quantitative differences are the following: (f) maximum amplitudes of ΔTEC disturbances are largest on D5 and lowest on D26, (h) maximum cross correlation occurs more toward eastward on D5-D6 while occurs more toward westward on D26-D27 and their velocities are higher than the velocities for D5 and D6.

Figure 7 represents the statistical evaluation of the MSTIDs characteristics for D5, D6, D26, and D27 in term of period, wavelength, and velocity, represented in blue, green, and red colors, respectively. The bars represent the standard deviation (STD) in the daily MSTID wave characteristics. The methodology used in the analyses is given in section 2.1.

It is possible to note the following important details in Figure 7: (g) The MSTIDs travel with a range of 155–189 m/s and with a wavelength range of 255–389 km in the S-N direction, while in the W-E direction these values are 122–142 m/s and 184–322 km. (h) The wave generally travels with higher velocity and larger wavelength in S-N direction than in W-E direction (i.e., MSTID travels faster equatorward for the four events). (i) Observing the variation of MSTID for each day from the error bar, it is possible to note that D27 represents the largest variation in their velocity, wavelength, and period. (j) The amplitudes of the daytime MSTIDs attain maximum during noon time which is a known characteristics [*Kotake et al.*, 2006; *Tsugawa et al.*, 2007; *Otsuka et al.*, 2013]. The polar plots of Figure 7 show clear evidence of the equatorward (or northward) directivity of the MSTID propagation for each wave event (left circle) and average for all events on each day (right circle). This shows consistency with the general properties of the MSTIDs observed.

4. Discussion

The characteristics (a-b) and (c-d) suggest that the oscillatory ΔTEC disturbances propagate equatorward/eastward in a form of wave which have periodicities ranging between 20 and 55 min and maximum amplitude during 13–16 UT. Periods and wavelengths of these ΔTEC disturbances are in same range as those of the MSTIDs, and therefore, they can be classified as the MSTIDs. These properties are in close agreement with past literatures on MSTIDs [*Hernandez-Pajares et al.*, 2006, 2012; *Tsugawa et al.*, 2007; *Otsuka et al.*, 2004, 2013; *Kotake et al.*, 2007, *MacDougall and Jayachandran*, 2011]. Taking *Hernandez-Pajares et al.* [2006, 2012] for reference, since part of their study deals with MSTID observations over Southern Hemisphere (at New Zealand), it is possible to note that the wave properties such as the velocity of propagation and wavelength varying from 100–400 m/s and 50–300 + km, respectively, are in good agreement with the present study. In addition, the daytime wave propagation direction in both studies are mainly to equatorward and eastward directions. The major contrast between these studies is that the daytime MSTIDs in the present study are observed during summer and solar moderate condition of December 2011 while most observations at *Hernandez-Pajares et al.* [2006, 2012] are during winter-fall daytime and spring-summer nighttime, but there were no major reports of MSTIDs occurrence during summer daytime for a complete solar cycle. *MacDougall and Jayachandran* [2011] using N_mF_2 from Southern Hemisphere shows daytime MSTIDs during summer and

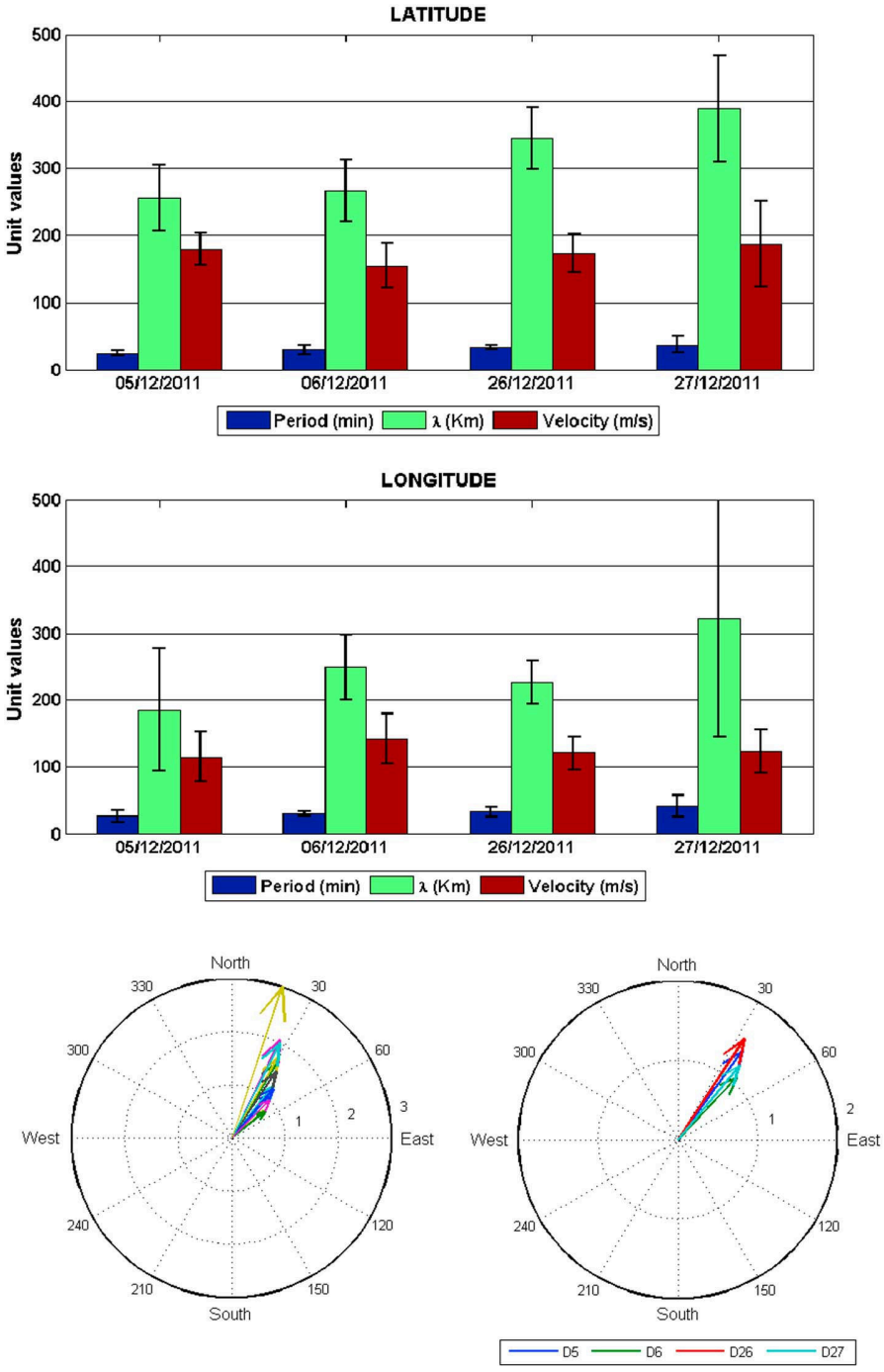

Figure 7. The statistical evaluation of the MSTIDs period, wavelength, and velocity, represented in blue, green, and red colors, respectively. The error bars represent the variance of daily MSTID wave characteristics. The polar plots at the bottom panels represent the directions of individual (left) and daily average (right) waves.

explain that daytime MSTIDs during summer should be expected since the AGW activity causing most daytime MSTIDs are approximately equal for both day and night.

The characteristic (e) suggests that these waves have S-N average wavelength longer than the W-E average wavelength. A close look into Figures 3 to 7 reveals that the S-N average wavelengths range between 255 and 389 km and is much longer than the W-E average wavelengths which range between 184 and 322 km.

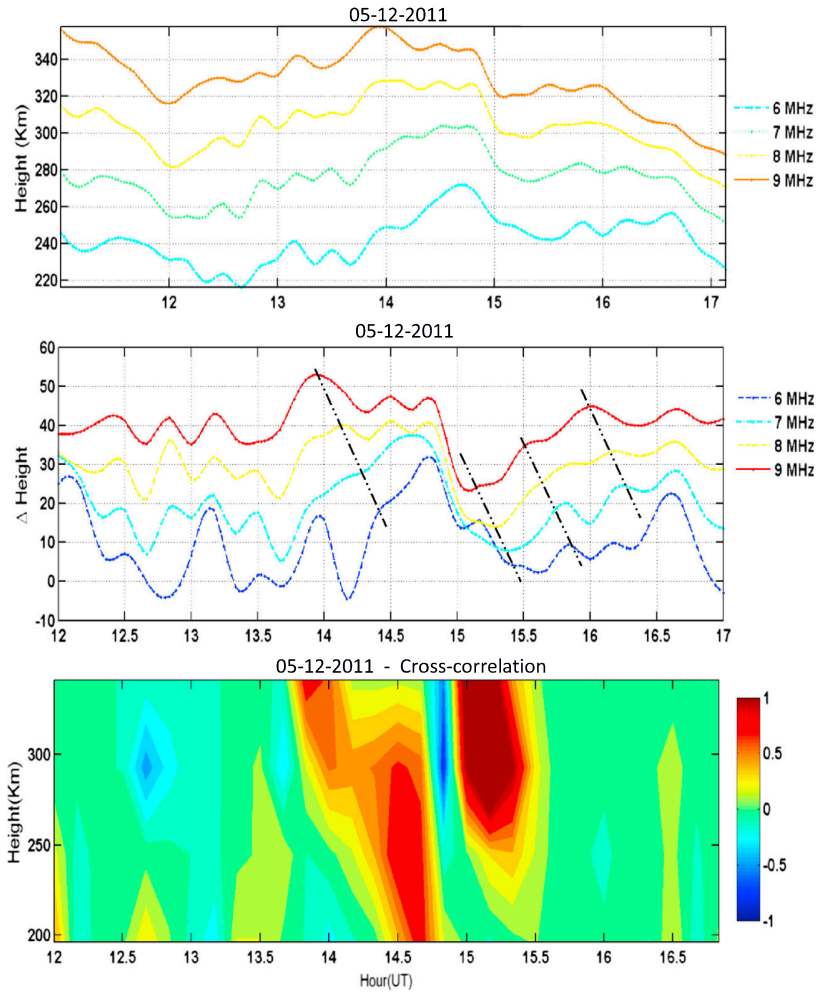

Figure 8. (top) The *hF* (height) of 6 to 9 MHz as a function of time, (middle) the Δheight, and (bottom) the cross-correlation coefficient map of Δheight in space and time using the same method of Figure 3.

Hence, the average propagation velocities are estimated at 187 and 122 m/s in the S-N and W-E directions, respectively. This observation shows that MSTIDs move faster toward equator than toward east. Therefore, this observation is a property of daytime MSTIDs which could be caused by the preferred movement of charge/neutral particles along geomagnetic field line compared to their orthogonal movement. This particular aspect suggests that the wavefronts of these daytime MSTIDs are inclined more toward S-N than W-E. In this appearance, they resemble the nighttime MSTIDs observed over Northern Hemisphere [*Tsugawa et al.*, 2007; *Otsuka et al.*, 2013] though they propagate eastward while the night-time MSTIDs propagate westward.

Another important outcome of the present study is that the southern MSTIDs are also preferentially propagating equatorward/eastward as shown by the polar plot at Figure 7 which is in agreement with the *Hernandez-Pajares et al.* [2006, 2012].

The equatorward propagation of MSTIDs as noted in this study and in earlier studies can be explained based on gravity wave forcing mechanism proposed by *Hooke* [1968]; *Kotake et al.* [2007]: the equatorward propagating gravity waves cause larger neutral particle oscillations in the north-south direction, in comparison to gravity waves propagating in other directions. This scenario leads to the larger ionospheric motion along geomagnetic field lines making the equatorward direction as a preferred direction of propagation for the MSTIDs. In the Southern Hemisphere over Brazil, owing to the large declination angle, aforementioned scenario may be slightly altered but still would maintain the same directivity which is consistent with the present study.

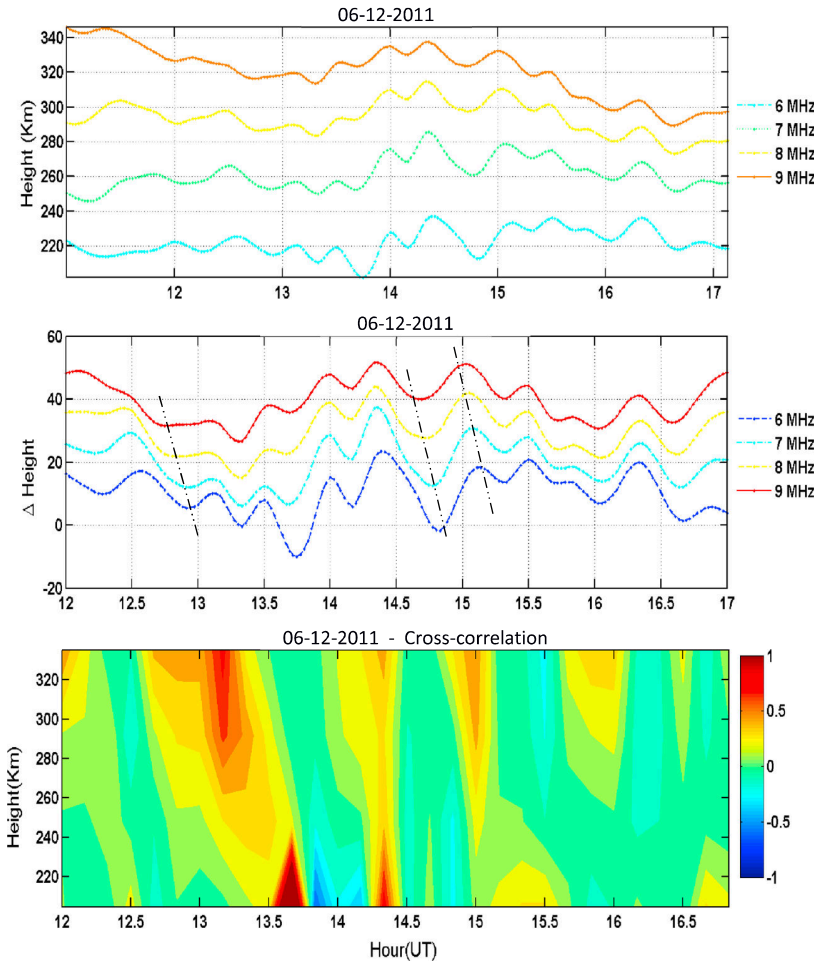

Figure 9. The same as Figure 8 but for day 6.

4.1. AGW Activity During D5 and D6

TIDs are known to be the manifestation of the atmospheric gravity waves (AGWs) arising either from underlying troposphere or from the auroral region [*Hunsucker*, 1982; *Huang et al.*, 1994; *Miller et al.*, 1997]. We use geomagnetic quiet days only to eliminate the forcing from auroral region. In recent years, the MSTIDs are observed during the tsunamis and they are diagnosed as owing to the AGWs forcing from below [*Makela et al.*, 2011; *Kherani et al.*, 2011]. Therefore, the AGWs are preferred forcing to generate the MSTIDs. The sources for the AGW have been proposed to be largely from upward propagating meteorological processes (e.g., orography and convection activities in the troposphere and stratosphere). Recently studies have attempted to provide various sources for AGW/TID. According to *MacDougall et al.* [2009b], AGWs could be driven by wind component along the magnetic field direction or through longitudinal mobility which are indirectly produced via convergence-divergence of ionization. The AGW can also be generated by the sunrise and sunset terminators [*MacDougall et al.*, 2009a] or be seeded by the Intertropical Convergence Zone [*MacDougall and Jayachandran*, 2011]. Hence, it is possible to infer that mechanisms causing AGW depend on the location, period, or season of the AGW/TIDs event. In the section that follows, we first show the signature of AGW during the same period of the observed MSTIDs as a clear link between AGW-MSTIDs and later investigate the possible mechanism responsible for the AGW generation.

According to *Lanchester et al.* [1993] and *Hocke and Schlegel* [1996], one can verify TID by looking at data from two frequencies and checking that they show downward phase motion. For this objective we selected a low-latitude to midlatitude station Cachoeira Paulista (45°W, 23°S, shown as red circle in Figure 1), and we examine the time variation of the ionospheric height observed by the digisonde during D5 and D6. Figures 8 and 9

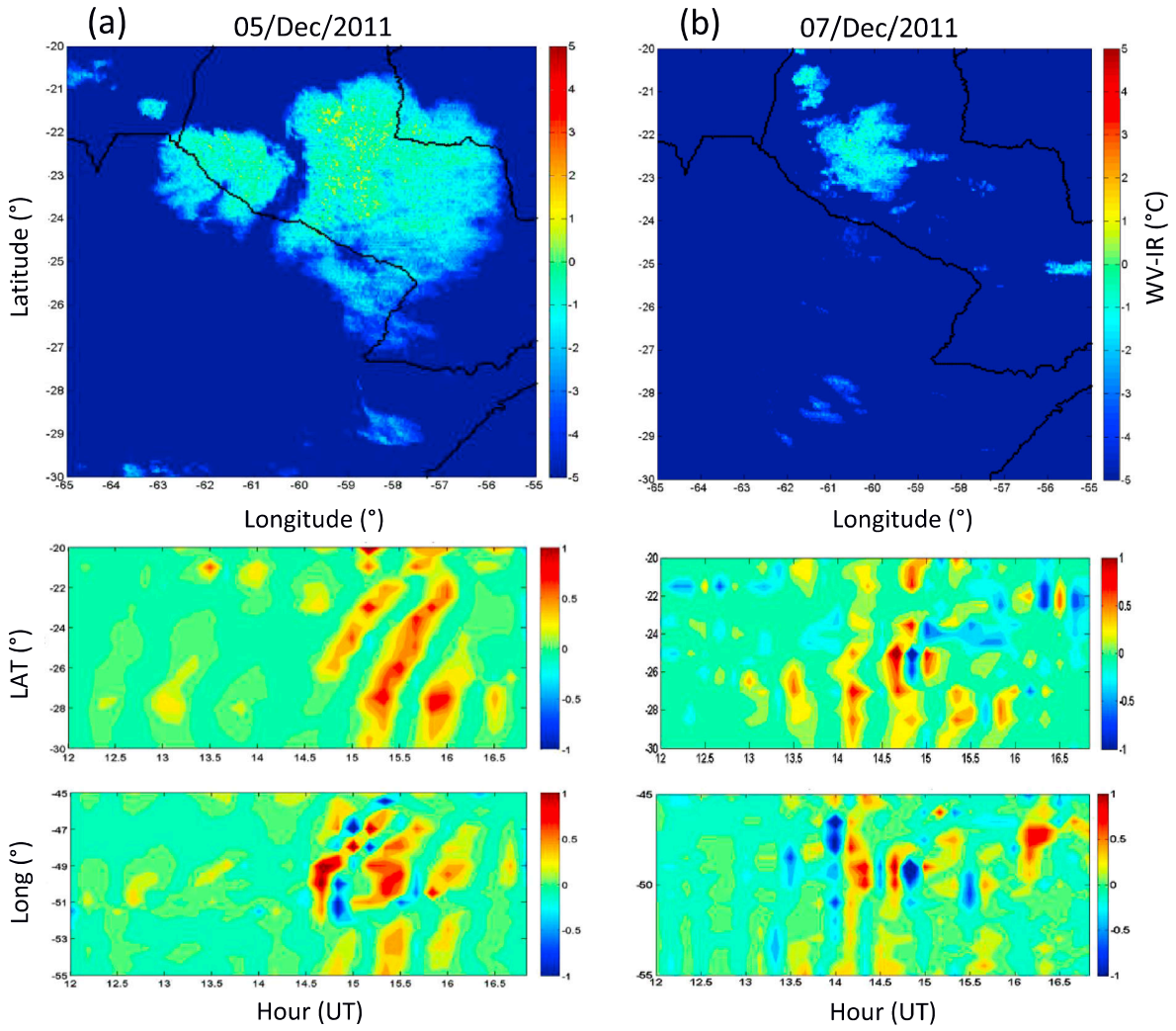

Figure 10. (a and b) Strong and weak convection with their corresponding MSTIDs propagations at the bottom panels.

present the results from the digisonde on these two days during 12–17 UT. In these figures, the top-to-bottom panels depict the temporal variation of the height (h) of the F region at 6–9 MHz frequencies, corresponding Δh variation, and the cross-correlation map of Δh, respectively. The Δh is defined as the h deviation from the best fitted (polynomial of order 7) h at each frequency.

From these figures, we note that the Δh acquires the oscillatory nature with large amplitude during 14–16 UT on D5 and during 13–15 on D6. Moreover, the cross correlation of Δh maximizes in these time intervals when the peak of Δh shifts downward as time progresses to the lower altitude suggesting the downward phase propagation of the wave responsible for the oscillation. The downward phase propagation is a unique characteristic of the upward propagating AGWs, and therefore, the noted oscillations of the height of the F region ionosphere during 14–16 UT on D5 and during 13–15 UT on D6 (see Figures 3 and 4) are caused by the upward propagating AGWs. We would like to point out that the MSTIDs begin to appear at 14 and 13 UT, respectively, on D5 and D6. Therefore, their appearance coincides with the appearance of the downward phase propagation of Δh. This is an important outcome of the present work which supports the possible association between AGWs and MSTIDs.

4.1.2. Possible AGW Mechanism and Coupling

As discussed in section 4.1, convective activity is one of the most important seeding for AGW. According to *Vadas et al.* [2009] deep clouds near the tropopause region are indicative of regions of active convection and

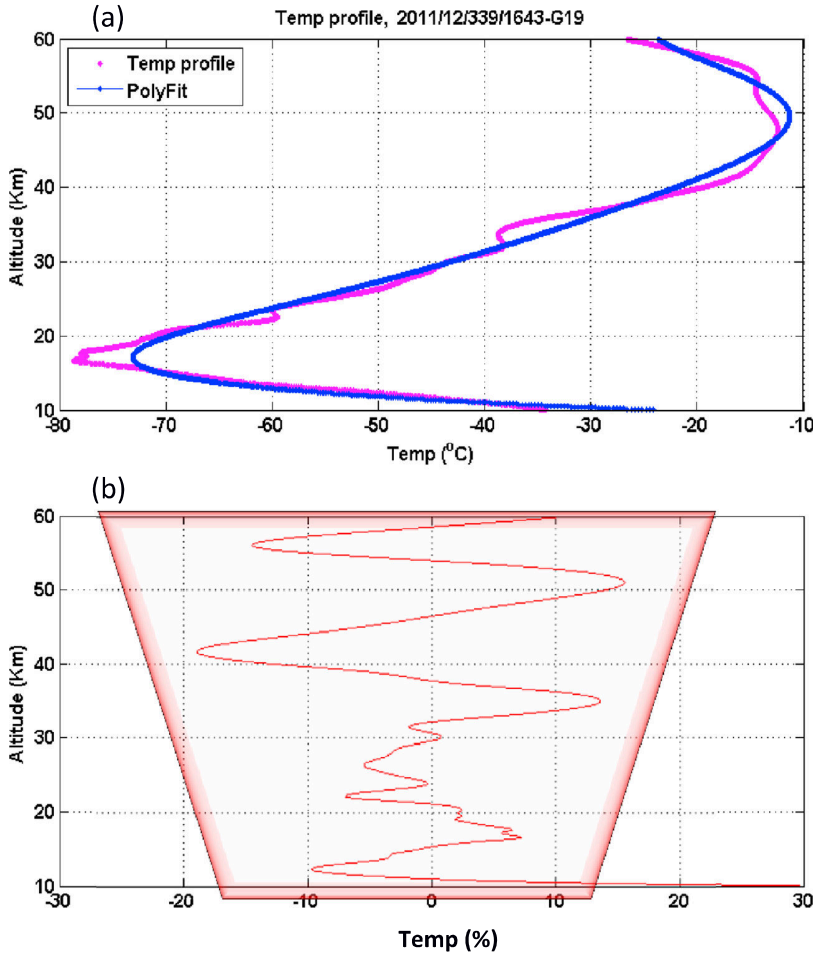

Figure 11. (a) Temperature profile COSMIC satellite (pink color) and its polynomial fit (blue color). (b) The signature of upward AGW propagation as obtained from the detrended temperature profile.

a likely source of gravity waves. Cold brightness temperature suggests deep convective plumes and convective overshoot which are a convenient launching platform for gravity waves [*Fritts et al.*, 2009]. AGW generated from the convective sources can propagate into the higher altitude and penetrate deep into the upper atmosphere [*Yigit et al.*, 2008; *Fritts et al.*, 2009]. In this subsection we extend our investigations on the findings of the enhanced MSTIDs around noon time due to AGW enhancement at the same time period as presented above. By using GOES 13 and COSMIC satellite data, we analyzed the tropospheric convective system on day 5 (strong convection) and day 7 (weak convection) in order to investigate the possible mechanism for AGW generation and provide evidence of the low atmosphere-ionosphere coupling.

Our convective activity is defined from the water vapor and infrared temperature data which are obtainable from the CPTEC/INPE web site. A strong convection activity implies that the difference in water vapor (WV) and infrared (IR) is greater than 0°C, i.e., WV − IR > 0°C, while a weak convection activity implies that WV − IR <°C.

We selected two days of strong convection (5 December 2011) and weak convection (7 December 2011) activities as shown in the top panels in Figures 10a and 10b. The deep and weak convection activities are seen very close to the site of the MSTIDs observation. By comparing the bottom panels in Figures 10a and 10b with the top panels, it is possible to clearly observe that MSTID on a strong convection day is much well defined than the MSTID on a weak convection day. This suggests clear evidence of convection activity as an important factor of AGW seeding.

Further evidence is shown by Figure 11 using the data from COSMIC satellite mission. The figure depicts the temperature profile obtained within the area (55°W–45°W, 30°S–20°S) under investigation. The blue and pink curves at Figure 11a represent the polynomial fit and temperature profile, respectively. The difference

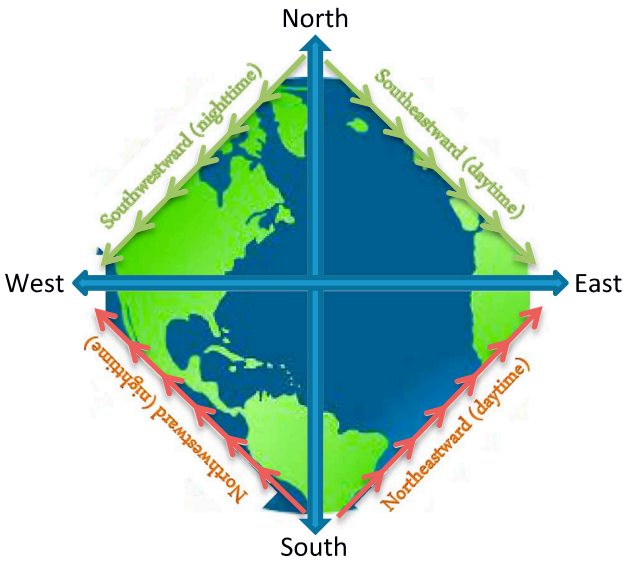

Figure 12. The green arrows represent the MSTIDs preferred directivity during nighttime (top left) and during daytime (top right) at the Northern Hemisphere; the red arrows represent the preferred directivity of MSTIDs during nighttime (bottom left) and during daytime (bottom right) at the Southern Hemisphere.

between the two curves is regarded as the detrended temperature profile which is represented at Figure 11b. From this figure it is possible to observe a major characteristic of AGW as seen in the amplitude increase with height. This is a clear signature of an upward AGW propagation. *Wang and Alexander* [2009] show that this type of structure from the COSMIC temperature data can be interpreted as signature of vertical gravity wave structure.. The AGW propagation upward from the troposphere (Figure 11) is possibly generated by the deep convection activity (Figure 10) on the day 5. Since the geomagnetic condition on this day was < 3, Joule heating and energetic particle precipitation are least expected to be an influence.

5. Conclusion

In the present study, we document MSTIDs over Southern Hemisphere during four days, 5, 6, 26, and 27 December 2011, by using the GNSS network, digisonde, GOES 13, and COSMIC satellite data. We examine the spatial-temporal distributions of total electron content (TEC) during 12–17 UT and covering the ionospheric domain of 30°S – 20°S latitude and 45° – 55°W longitude. The investigations into the mechanism responsible for the AGW-MSTIDs are also carried out.

For the TEC data, we derive the ΔTEC disturbance by subtracting the TEC mean from corresponding best fitted (TEC_{fit}) obtained using polynomial fit of order 7.

This fitting is done in time and the temporal variation of ΔTEC is derived at several locations within the ionospheric domain to generate the keogram of TEC. Furthermore, cross-correlation keograms of these spatially distributed ΔTEC are obtained in latitude and longitude.

These keograms suggest that the ΔTEC disturbances acquire the wave characteristics during 13–16 UT that propagate equatorward/eastward having S-N average wavelength in the 255–389 km range and W-E average wavelength in the 184–322 km range. These characteristics classify the ΔTEC disturbances as MSTIDs resembling the MSTIDs characteristics widely reported over Northern Hemisphere.

This study also reports strong summer daytime MSTIDs occurrence for four days during December 2011 using detrended TEC parameter, which was not observed before over Southern Hemisphere. Other past studies at this region have only identified winter daytime MSTID occurrence.

A possible connection between the observed MSTIDs and gravity waves is examined by analyzing the temporal variation of the *F* region height (*h*) inferred from digisonde over a low-latitude to midlatitude station on 5 and 6 December 2011. We derive the Δh by subtracting the h from its best fitted (h_{fit}) at 6, 7, 8, and 9 MHz and also obtained the cross-correlation map of height distribution of *h*. They show the maximum cross correlation occurring between 13 and 16 UT also revealing the downward phase propagation in time suggesting the enhanced gravity wave activity during the time when MSTIDs are observed. These characteristics are found to be similar on day-to-day basis; however, numerical simulations are needed to justify these observations.

Our results show a close correlation between enhanced MSTIDs and AGW during daytime and bring out the issue about the convection activity as AGW generation.

We show cloud convection activity as an important factor of AGW-MSTIDs generation during daytime between the hours of 12 to 17 UT for the analyzed days. Results presented in this study also show a clear

observation of upward propagating AGW from lower atmosphere to upper atmosphere which is important for atmosphere-ionosphere coupling.

Although, nighttime MSTIDs are associated with electrodynamics processes and the daytime MSTIDs are related to AGW, it should be mentioned that the nighttime MSTIDs in the Northern and Southern Hemispheres propagate in same direction, i.e., equatorward-westward, and this same hemispheric directivity (as shown in Figure 12) is explained as due to the geomagnetic conjugate dynamics [*Otsuka et al.*, 2004]. For the daytime MSTIDs, with the input from our present study and *Hernandez-Pajares et al.* [2006, 2012], it is clear that these MSTIDs propagate to the same direction in both hemispheres. Therefore, similar hemispheric directivity (as shown in Figure 12) for the daytime MSTIDs can possibly also be attributed to the geomagnetic conjugate dynamics. This possibility can only be examined by simultaneous observation and simulation of daytime MSTIDs over both hemispheres in future work.

Acknowledgments

We appreciate the availability of data at the following data bases: The Brazilian Network for Continuous Monitoring (RBMC/IBGE), the Geostationary Operational Environmental Satellite system (GOES) manage by CPTEC/INPE, Constellation Observing System for Meteorology, Ionosphere, and Climate (COSMIC).. O.F. Jonah and E.R. de Paula would like to acknowledge the supports from Conselho Nacional de Desenvolvimento Científico e Tecnológico (CNPq) under process 133429/2011-3 and 305684/2010-8 grants, respectively. E.A. Kherani is grateful to FAPESP under process 2011/21903-3. The authors also acknowledge Inez Batista for the digisonde data.

References

Amorim, D. C. M., A. A. Pimenta, J. A. Bittencourt, and P. R. Fagundes (2011), Long term study of medium scale traveling ionospheric disturbances using O I 630 nm all sky imaging and ionosonde over Brazilian low latitudes, *J. Geophys. Res.*, *116*, A06312, doi:10.1029/2010JA016090.

Bristow, W. A., and R. A. Greenwald (1996), Multiradar observations of medium-scale acoustic gravity waves using the Super Dual Auroral Radar Network, *J. Geophys. Res.*, *101*, 24,499–24,511, doi:10.1029/96JA01494.

Candido, C. M. N., A. A. Pimenta, J. A. Bittencourt, and F. Becker-Guedes (2008), Statistical analysis of the occurrence of medium-scale traveling ionospheric disturbances over Brazilian low latitudes using OI 630.0 nm emission all-sky images, *Geophys. Res. Lett.*, *35*, L17105, doi:10.1029/2008GL035043.

Chen, X., H. Landau, and U. Vollath (2003), New tools for network RTK integrity monitoring paper presented at ION GPS/2003, Inst. of Navig., Portland, Oreg.

Fritts, D. C., et al. (2009), Overview and summary of the Spread *F* Experiment (SpreadFEx), *Ann. Geophys.*, *27*, 2141–2155, doi:10.5194/angeo-27-2141-2009.

Galvan, D. A., A. Komjathy, M. P. Hickey, and A. J. Mannucci (2011), The 2009 Samoa and 2010 Chile tsunamis as observed in the ionosphere using GPS total electron content, *J. Geophys. Res.*, *116*, A06318, doi:10.1029/2010JA016204.

Grocott, A., K. Hosokawa, T. Ishida, M. Lester, S. E. Milan, M. P. Freeman, N. Sato, and A. S. Yukimatu (2013), Characteristics of medium-scale traveling ionospheric disturbances observed near the Antarctic Peninsula by HF radar, *J. Geophys. Res. Space Physics*, *118*, 5830–5841, doi:10.1002/jgra.50515.

Hernandez-Pajares, M., J. M. Juan, and J. Sanz (2006), Medium-scale traveling ionospheric disturbances affecting GPS measurements: Spatial and temporal analysis, *J. Geophys. Res.*, *111*, A07S11, doi:10.1029/2005JA011474.

Hernández-Pajares, M., J. M. Juan, J. Sanz, and A. Aragón-Àngel (2012), Propagation of medium scale traveling ionospheric disturbances at different latitudes and solar cycle conditions, *Radio Sci.*, *47*, RS0K05, doi:10.1029/2011RS004951.

Hines, C. O. (1960), Internal atmospheric gravity waves at ionospheric heights, *Can. J. Phys.*, *38*, 1441–1481.

Hocke, K., and K. A. Schlegel (1996), Review of atmospheric gravity waves and travelling ionospheric disturbances: 1982–1995, *Ann. Geophys.*, *14*, 917–940, doi:10.1007/s00585-996-0917-6.

Hooke, W. H. (1968), Ionospheric irregularities produced by internal atmospheric gravity waves, *J. Atmos. Sol. Terr. Phys.*, *30*, 795–823.

Huang, C. S., C. A. Miller, and M. C. Kelley (1994), Basic properties and gravity wave initiation of the midlatitude *F* region instability, *Radio Sci.*, *29*(l), 395–405, doi:10.1029/93RS01669.

Hunsucker, R. (1982), Atmospheric gravity waves generated in the high latitude ionosphere: A review, *Rev. Geophys. Space Phys.*, *20*, 293–315.

Jonah, O. F., E. R. de Paula, E. A. Kherani, S. L. G. Dutra, and R. R. Paes (2014), Atmospheric and ionospheric response to stratospheric sudden warming of January 2013, *J. Geophys. Res. Space Physics*, *119*, 4973–4980, doi:10.1002/2013JA019491.

Jonah, O. F., E. R. de Paula, M. T. A. H. Muella, S. L. G. Dutra, E. A. Kherani, P. M. S. Negreti, and Y. Otsuka (2015), TEC variation during high and low solar activities over South American sector, *J. Atmos. Sol. Terr. Phys.*, *135*, 22–35, doi:10.1016/j.jastp.2015.10.005.

Kelley, M. C. (2011), On the origin of mesoscale TIDs at midlatitudes, *Ann. Geophys.*, *29*, 361–366, doi:10.5194/angeo-29-361.

Kherani, E. A., M. A. Abdu, D. Fritts, and E. R. de Paula (2011), The acoustic gravity wave induced disturbances in the equatorial ionosphere, in *Aeronomy of the Earth's Atmosphere and Ionosphere*, *IAGA Spac. Soporan Book Ser.*, edited by M. A. Abdu, D. Pancheva, and A. Bhattacharyya, pp. 141–162, Springer, Kiruna, Sweden.

Kotake, N., Y. Otsuka, T. Tsugawa, T. Ogawa, and A. Saito (2006), Climatological study of GPS total electron content variations caused by medium-scale traveling ionospheric disturbances, *J. Geophys. Res.*, *111*, A04306, doi:10.1029/2005JA011418.

Kotake, N., Y. Otsuka, T. Tsugawa, T. Ogawa, and A. Saito (2007), Statistical study of medium-scale traveling ionospheric disturbances observed with the GPS networks in Southern California, *Earth Planets Space*, *59*, 95–102.

Lanchester, B. S., T. Nygren, M. J. Jarvis, and R. Edwards (1993), Gravity wave parameters measured with EISCAT and Dynasonde, *Ann. Geophys.*, *11*, 925–936.

MacDougall, J. W., and P. T. Jayachandran (2011), Spaced transmitter measurements of medium scale traveling ionospheric disturbance near equator, *Geophys. Res. Lett.*, *38*, L16806, doi:10.1029/2011GL048598.

MacDougall, J., G. Li, and P. T. Jayachandran (2009a), Traveling ionospheric disturbances near London, Canada, *J. Atmos. Sol. Terr. Phys.*, *71*, 2077–2084, doi:10.1016/j.jastp.2009.09.016.

MacDougall, J., M. Abdu, I. Batista, P. R. Fagundes, Y. Sahai, and P. T. Jayachandran (2009b), On the production of traveling ionospheric disturbances by atmospheric gravity waves, *J. Atmos. Sol. Terr. Phys.*, *71*, 2013–2016, doi:10.1016/j.jastp.2009.09.006.

Makela, J. J., et al. (2011), Imaging and modeling the ionospheric airglow response over Hawaii to the tsunami generated by the Tohoku earthquake of 11 March 2011, *Geophys. Res. Lett.*, *38*, L00G02, doi:10.1029/2011GL047860.

Miller, E. S., W. E. Swartz, M. C. Kelley, M. Mendillo, D. Nottingham, J. Scali, and B. Reinisch (1997), Electrodynamics of midlatitude spread *F*, 1. Observations of unstable, gravity wave-induced ionospheric electric fields at tropical latitudes, *J. Geophys. Res.*, *102*, 11,521–11,532, doi:10.1029/96JA03839.

Miller, E. S., H. Kil, J. J. Makela, R. A. Heelis, E. R. Talaat, and A. Gross (2014), Topside signature of medium-scale traveling ionospheric disturbances, *Ann. Geophys.*, *32*, 959–965, doi:10.5194/angeo-32-959-2014.

Nicolls, M. J., and M. C. Kelley (2005), Strong evidence for gravity wave seeding of an ionospheric plasma instability, *Geophys. Res. Lett.*, *32*, L05108, doi:10.1029/2004GL020737.

Nogueira, P. A. B., M. A. Abdu, J. R. Souza, G. J. Bailey, and I. S. Batista (2013), Longitudinal variation in Global Navigation Satellite Systems TEC and topside ion density over South American sector associated with the four-peaked wave structures, *J. Geophys. Res. Space Physics*, *118*, 1–14, doi:10.1002/2013JA019266.

Oliver, W. L., Y. Otsuka, M. Sato, T. Takami, and S. Fukao (1997), A climatology of *F*-region gravity wave propagation over the middle and upper atmosphere radar, *J. Geophys. Res.*, *102*, 14,499–14,512, doi:10.1029/97JA00491.

Otsuka, Y., T. Ogawa, A. Saito, T. Tsugawa, S. Fukao, and S. Miyazaki (2002), A new technique for mapping of total electron content using GPS network in Japan, *J. Earth Planets Space*, *54*, 63–70.

Otsuka, Y., K. Shiokawa, T. Ogawa, and P. Wilkinson (2004), Geomagnetic conjugate observations of medium-scale traveling ionospheric disturbances at midlatitude using all-sky airglow imagers, *Geophys. Res. Lett.*, *31*, L15803, doi:10.1029/2004GL020262.

Otsuka, Y., Kotake, N., Shiokawa, K., T. Ogawa, T. Tsugawa, and A. Saito (2011), Statistical study of medium-scale traveling ionospheric disturbances observed with a GPS receiver network in Japan, in *Aeronomy of the Earth's Atmosphere and Ionosphere*, *IAGA Spec. Sopron Book Ser.*, vol. 2, pp. 291–299, Springer, Netherlands, doi:10.1007/978-94-007-0326-121.

Otsuka, Y., K. Suzuki, S. Nakagawa, M. Nishioka, K. Shiokawa, and T. Tsugawa (2013), GPS observations of medium-scale traveling ionospheric disturbances over Europe, *Ann. Geophys.*, *31*(163–172), 2013, doi:10.5194/angeo-31-163.

Paes, R. R., I. S. Batista, C. M. N. Candido, O. F. Jonah, and P. C. P. Santos (2014), Equatorial ionization anomaly variability over the Brazilian region during boreal sudden stratospheric warming events, *J. Geophys. Res. Space Physics*, *119*, 7649–7664, doi:10.1002/2014JA019968.

Pimenta, A. A., M. C. Kelley, Y. Sahai, J. A. Bittencourt, and P. R. Fagundes (2008), Thermospheric dark band structures observed in all-sky OI 630 nm emission images over the Brazilian low-latitude sector, *J. Geophys. Res.*, *113*, A01307, doi:10.1029/2007JA012444.

Takahashi, H., et al. (2014), Diagnostics of equatorial and low latitude ionosphere by TEC mapping over Brazil, *Adv. Space Res.*, *54*, 385–394, doi:10.1016/j.asr.2014.01.032.

Tsugawa, T., Y. Otsuka, A. J. Coster, and A. Saito (2007), Medium-scale traveling ionospheric disturbances detected with dense and wide TEC maps over North America, *Geophys. Res. Lett.*, *34*, L22101, doi:10.1029/2007GL031663.

Vadas, S. L., M. J. Taylor, P.-D. Pautet, P. A. Stamus, D. C. Fritts, H.-L. Liu, F. T. São Sabbas, V. T. Rampinelli, P. Batista, and H. Takahashi (2009), Convection: The likely source of the medium-scale gravity waves observed in the OH airglow layer near Brasilia, Brazil, during the SpreadFEx campaign, *Ann. Geophys.*, *27*, 231–259, doi:10.5194/angeo-27-231.

Wanninger, L. (2004), Ionospheric disturbance indices for RTK and network RTK positioning paper presented at ION GPS/2004, Inst. of Navig., Long Beach, Calif.

Wang, L., and J. Alexander (2009), Gravity wave activity during stratospheric sudden warming in the 2007-2008 Northern Hemisphere winter, *J. Geophys. Res.*, *114*, doi:10.1029/2009JD011867.

Yigit, E., A. D. Aylward, and A. S. Medvedev (2008), Parameterization of the effects of vertically propagating gravity waves for thermosphere general circulation models: Sensitivity study, *J. Geophys. Res.*, *113*, D19106, doi:10.1029/2008JD010135.